IEEE Access
Multidisciplinary ⋮ Rapid Review ⋮ Open Access Journal

Received December 16, 2019, accepted January 15, 2020, date of publication January 20, 2020, date of current version January 30, 2020.

Digital Object Identifier 10.1109/ACCESS.2020.2967835

A Control Parameter Design Method for Hybrid Multi-Terminal HVDC System

BINGKUN LI, YUANSHENG LIANG, GANG WANG, HAIFENG LI, AND XINQUAN CHEN
School of Electric Power Engineering, South China University of Technology, Guangzhou 510641, China

Corresponding author: Yuansheng Liang (ysliang@scut.edu.cn)

This work was supported by the National Natural Science Foundation of China under Grant 51577072.

ABSTRACT To achieve better control performance, a comprehensive control parameter design method that considers economics, stability and dynamic performance is essential for hybrid multi-terminal HVDC systems. In this paper, a hierarchical model for the control system of Hybrid-MTDC is constructed and the parameters are optimized on two layers. On the system layer, using the normalization processing method, a system-layer objective function that considers both the minimum network loss and the voltage offset is formed for Hybrid-MTDC systems and solved with the proposed penalty interior point method. On the converter layer, using the state-space matrix method, a generic small-signal stability range of each control parameter can be obtained by the traversal calculation of the eigenvalues. Then, to identify the stricter stable operating region for the DC voltage controller under severe conditions, an additional stability criterion based on the mixed-potential theory is deduced, and the design-oriented boundaries are generated and added to the feasible region. Finally, within the design-oriented boundaries, a general dynamic performance evaluation function is constructed to determine the optimal control parameters. Utilizing the proposed method, a typical Hybrid-MTDC system is investigated, and experimental verifications are provided to validate the effectiveness and accuracy.

INDEX TERMS Hybrid multi-terminal HVDC systems, comprehensive control parameter design method, minimum network loss, voltage offset, additional stability criterion, dynamic performance evaluation.

I. INTRODUCTION

In traditional HVDC projects, line commutation converters (LCC) have benefits such as high transmission capacity and low cost [1], [2]. As a new transmission technology, the multi-level modular converter (MMC), with the advantages of reduced harmonics and good controllability, is becoming a viable alternative for HVDC transmission [3]–[5]. In 2018, combining the advantages of both LCCs and MMCs, the world's first hybrid 3-terminal HVDC system was construction in the China Southern Grid [6]. Hybrid multi-terminal HVDC (Hybrid-MTDC) transmission systems have become an important topic in power industry development [5]–[7]. The selection of the control parameters for Hybrid-MTDC systems determines the economics, stability and efficiency of the system.

Most control parameter designs in engineering rely on a trial-and-error approach or an electromagnetic transient software optimization program, which is time consuming and cannot guarantee that the system will run under optimal conditions or even stably [8], [9]. Hence, it is of great significance to find an efficient and comprehensive method for designing the control parameters to ensure stability and excellent performance. Recently, many scholars have conducted extensive research on HVDC systems. Based on the well-known steady-state equations of LCCs, a small-signal dynamic model of an LCC-HVDC system was developed [10], [11]. References [12]–[16] employed an average-value model of MMCs, investigating the oscillatory modes of the system. References [17]–[19] focused on the small-signal stability analysis of hybrid HVDC systems, analysing the influence of the PI control parameters. However, for the control parameter design of Hybrid-MTDC systems, there are several issues remained as follows:

1) Control parameter design on the system layer: Different from traditional HVDC networks, since Hybrid-MTDC systems contain more converter stations and more complex network topologies [17]–[19], there might be many scenarios of power flow control on the system layer. However, the existing literature [17]–[19] ignores

The associate editor coordinating the review of this manuscript and approving it for publication was Tariq Masood.

control parameter analyses on the system layer. The power flow control parameters on the system layer affect network losses and voltage offsets, which determines the economics of operating Hybrid-MTDC systems in the steady state.

2) Additional stability criterion under severe conditions: The DC voltage control is the most important control target in Hybrid-MTDC systems and determines the stable operation of the whole system [6]. In engineering, more stringent and specific stability and performance requirements for the DC voltage controller are essential to guarantee reliable operation. However, the traditional small-signal stability analysis is only applicable to system estimations under weak disturbances [10]–[19] and fails to describe how much disturbance the control parameters satisfying the small-signal stability request can withstand [20]. This obviously does not meet the stringent requirements for critical DC voltage controllers in engineering.
3) Efficient global dynamic performance analysis: Reference [18] proposed a quantitative dynamic performance evaluation for Hybrid-MTDC systems based on a time-domain mathematical model. However, this method can only perform an inverse Laplace transform for one of the outputs to analyse the dynamic indicators, which cannot be used as the global optimal term for all outputs of the dynamic performance analysis. Hence, this method fails to solve the global optimal control parameters of the system.

Therefore, to propose a comprehensive control parameter design method for Hybrid-MTDC systems, the main contributions of this paper are listed as follows:

(i) Considering the economics of operating Hybrid-MTDC systems in the steady state, an objective function on the system layer that includes both the minimum network loss and the voltage offset is formed for Hybrid-MTDC systems. The power balance of the DC network and the voltage limit of the DC node are used as constraints. Then, the penalty interior point method is constructed as a fast solution method to ensure that the power flow control of the Hybrid-MTDC system is at the target optimal state under steady state operation.

(ii) Using the state-space matrix method, a generic small-signal stability range for each control parameter can be obtained by the traversal calculation of the eigenvalues. Then, to identify the stricter stable operating region for the DC voltage controller under severe conditions, an additional stability analysis based on the mixed-potential theory is performed and the design-oriented boundaries are generated and added to the feasible region.

(iii) Within the design-oriented boundaries, a dynamic performance evaluation function is constructed using the damping ratio and the negative real part of the eigenvalue, which can describe the dynamic performance of all oscillation modes of the system. Thus, a comprehensive control parameter design method for Hybrid-MTDC systems is proposed considering the optimal state under steady state operation, the small-signal stability of all control parameters, additional stability criterion for DC voltage controllers and the optimal dynamic performance.

Finally, experimental verifications are provided to validate the effectiveness and accuracy of the proposed method.

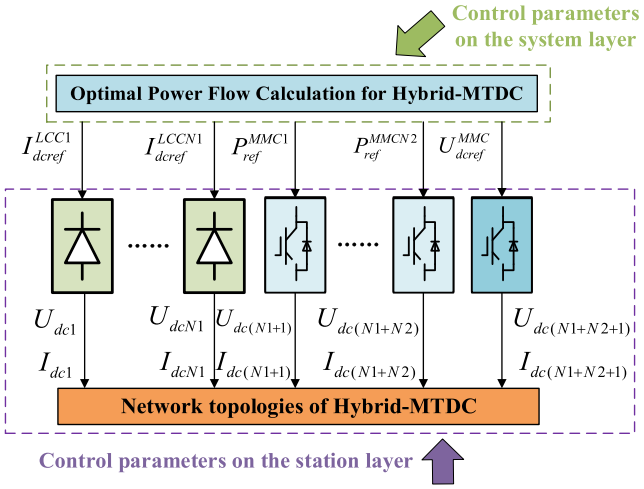

FIGURE 1. Hierarchical schematic diagram for the control of Hybrid N-terminal HVDC transmission systems.

II. COMPREHENSIVE CONTROL PARAMETER DESIGN METHOD FOR HYBRID MULTI-TERMINAL HVDC SYSTEMS

A. OPTIMAL POWER FLOW CONTROL ON THE SYSTEM LAYER

Hybrid-MTDC systems include LCC and MMC stations. To take advantage of the large capacity of the LCC stations, LCCs generally work in current control mode and the MMC station with the largest capacity is used to control the DC voltage, while the other stations control the active power [21]. This control strategy is conducive to ensuring that the power system runs in a stable and economical state [22]. In this paper, the power control system of the Hybrid-MTDC is divided into two parts as shown in Fig. 1, consisting of a system layer and converter station layers. The system layer sends the reference control parameters to each converter station through the fibre channel. Following that, the control system of each converter station is adjusted according to the received control parameters. Simultaneously, the local DC voltage and the active power signal are collected and fed back to the upper control system.

On the system layer, with the minimum network loss as the primary condition for controlling the target, the corresponding objective function f_1 can be obtained as follows:

$$f_1(x) = -\sum_{i=1}^{N1+N2+1}\sum_{j=i+1}^{N1+N2+1} G_{ij}(U_{dci} - U_{dcj})^2 = \sum_{i=1}^{N1+N2+1} P_i \tag{1}$$

where G_{ij} is the mutual conductance between node i and j; (N1+N2+1) is the number of DC nodes; P_i is the active

power transmitted by the i-th station; U_{dc} is the voltage of the DC node; and the direction from the AC system into the DC grid is positive.

Considering the importance of DC voltage in the stable operation of Hybrid-MTDC grids, the minimum deviation of DC voltage is added as the objective function f_2:

$$f_2(x) = \sum_{i=1}^{N1+N2+1} \sqrt{(U_{dci} - U_{dci}^*)^2} \tag{2}$$

where U_{dci}^* is the DC voltage expectation value of node i.

To consider the two different control objectives (1) and (2), this paper introduces a normalized method to construct the optimal objective function of the system control layer:

$$f(x) = \omega_1 \cdot \frac{-\sum_{i=1}^{N1+N2+1}\sum_{j=1}^{N1+N2+1} G_{ij}(U_{dci} - U_{dcj})^2}{P_{loss}^{\max}} + \omega_2 \cdot \frac{1}{(N1+N2+1)} \cdot \sum_{i=1}^{N1+N2+1} \frac{\sqrt{(U_{dci} - U_{dci}^*)^2}}{(U_{dci}^{\max} - U_{dci}^{\min})} \tag{3}$$

where $\boldsymbol{x}$=[U_{dc1}, U_{dc2},……, $U_{dc(N1+N2+1)}$]; ω_1 represents the weight factor of network loss; ω_2 is the weight factor of the nodal voltage offset; $P_{loss}^{\max}$ is the maximum loss value of the DC network; And $U_{dci}^{\max}$ and $U_{dci}^{\min}$ are the allowable range of the node DC voltage.

The power balance of the transmission lines is introduced as the equality constraint $\boldsymbol{h}(\boldsymbol{x})$, and the capacity and voltage limits of the stations is the inequality constraint $\boldsymbol{g}(\boldsymbol{x})$. Hence, the optimization model for optimal power flow control on the system layer can be obtained as follows:

$$\begin{cases} \min f(x) \\ \quad = \omega_1 \cdot \dfrac{-\sum_{i=1}^{N1+N2+1}\sum_{j=1}^{N1+N2+1} G_{ij}(U_{dci} - U_{dcj})^2}{P_{loss}^{\max}} \\ \quad +\omega_2 \cdot \frac{1}{(N1+N2+1)} \cdot \sum_{i=1}^{N1+N2+1} \dfrac{\sqrt{(U_{dci} - U_{dci}^*)^2}}{(U_{dci}^{\max} - U_{dci}^{\min})} \\ s.t. \begin{cases} h_i(x) = P_i - U_{dci} \sum_{k\in\{k|\text{nodes connected to } i\}} G_{ik} U_{dck} = 0 \\ \qquad i = 1, 2 \ldots, N1+N2+1 \\ g_{li} = U_{dci}^{\min} \le g_i(x) = U_{dci} \le g_{hi} = U_{dci}^{\max} \\ \qquad i = 1, 2 \ldots, N1+N2+1 \\ g_{lj} = P_j^{\min} \le g_j(x) = P_j \le g_{hj} = P_j^{\max} \\ \qquad j = 1, 2 \ldots, N1+N2+1 \end{cases} \end{cases} \tag{4}$$

To ensure efficient computational efficiency and numerical robustness, the penalty interior point method is used for calculation. The relaxation quantity is introduced to relax the equality constraint and inequality constraint, and then the model is transformed as follows:

$$L = f(x) - \boldsymbol{y}^T\boldsymbol{h}(\boldsymbol{x}) - \boldsymbol{z}^T[\boldsymbol{g}(\boldsymbol{x}) - \boldsymbol{l} - \boldsymbol{g_l}] \cdot \boldsymbol{w}^T[\boldsymbol{g}(\boldsymbol{x}) + \boldsymbol{u} - \boldsymbol{g_h}] - \mu\sum_{i=1}^{r}\ln(l_j) - \mu\sum_{i=1}^{r}\ln(u_j) \tag{5}$$

where $\boldsymbol{y}$ = [y_1,……, $y_{N1+N2+1}$]$^{\mathrm{T}}$ represents the Lagrange multipliers of the equality constraints; $\boldsymbol{z}$ = [z_1,……, $z_{2(N1+N2+1)}$]$^{\mathrm{T}}$ and $\boldsymbol{w}$ = [w_1,……, $w_{2(N1+N2+1)}$]$^{\mathrm{T}}$ are the Lagrange multipliers of the inequality constraints; $\boldsymbol{l}$ = [l_1, ……,$l_{2(N1+N2+1)}$]$^{\mathrm{T}}$ and $\boldsymbol{u}$ = [u_1,……, $u_{2(N1+N2+1)}$]$^{\mathrm{T}}$ are the relaxation variables with inequality constraints; and μ is the penalty factor.

Following that, according to the preset weight value, the Kuhn-Tucker condition (KKT) and the approximate correction equation, listed at Appendix (A1)-(A6), are used to calculate the optimal power flow of the DC grid. The designed control parameters ($\boldsymbol{I}_{dcref}^{LCC}$, $\boldsymbol{P}_{ref}^{MMC}$, $\boldsymbol{U}_{dcref}^{MMC}$) are issued to each converter station layer.

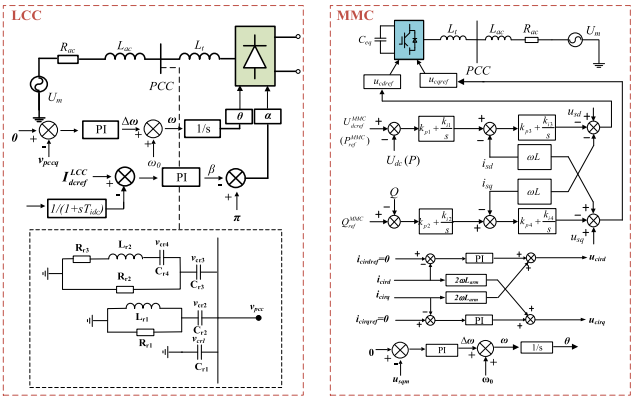

FIGURE 2. Equivalent converters and controllers in the stations.

B. SYSTEM MODELING AND FEASIBLE CONTROL PARAMETER REGIONS UNDER SMALL-SIGNAL STABILITY

According to the calculation in *part. A*, the optimal power flow control parameters on the system layer can be determined. Following that, to clarify the Hybrid-MTDC system mathematically, the LCC and MMC mathematical models can be described by the switching function method [18]. The LCC equivalent models and the MMC equivalent mathematical models, including the control system, are constructed in Appendix (B1)-(B3) and (B4)-(B11). The general model of the DC network in the Hybrid-MTDC system is deduced in (B12). The schematic diagram of the converter stations and corresponding control systems is depicted in Fig. 2, and the physical meanings of the variables are listed in Tab. 1.

To facilitate the expression of the system model, the subscripts $\boldsymbol{X}_{Idc/P/Udc/dcl}$ are used to distinguish the function type of the converter stations, while the superscripts $\boldsymbol{X}^{LCCi/MMCj}$ are used to distinguish the number of the converter stations. From (B1)-(B12), the state vectors of the Hybrid-MTDC

TABLE 1. Physical meanings of the variables.

Vector	Physical meaning	Variables
$\boldsymbol{X}_{Idc}^{LCCi}$ (i=1,2…N1)	PCC voltage	$v_{pccd}^{(LCCi)}$, $v_{pccq}^{(LCCi)}$
	AC filter	$v_{cr2d}^{(LCCi)}$, $v_{cr2q}^{(LCCi)}$, $i_{Lr1d}^{(LCCi)}$, $i_{Lr1q}^{(LCCi)}$, $v_{cr3d}^{(LCCi)}$, $v_{cr3q}^{(LCCi)}$, $v_{cr4d}^{(LCCi)}$, $v_{cr4q}^{(LCCi)}$, $i_{Lr2d}^{(LCCi)}$, $i_{Lr2q}^{(LCCi)}$,
	AC current	$i_{sd}^{(LCCi)}$, $i_{sq}^{(LCCi)}$
	DC current controller	$I_{derm}^{(LCCi)}$, $I_{dci}^{(LCCi)}$
	PLL	$x_{PLL}^{(LCCi)}$, $\omega^{(LCCi)}$
$\boldsymbol{X}_{P}^{MMCj}$ (j=1,2…N2) $\boldsymbol{X}_{Udc}^{MMCj}$ (j=N2+1)	PCC voltage	$u_{sd}^{(MMCj)}$, $u_{sq}^{(MMCj)}$
	AC current	$i_{sd}^{(MMCj)}$, $i_{sq}^{(MMCj)}$
	DC voltage component of SM capacitor	$u_{C\_dc}^{(MMCj)}$
	1st voltage component of SM capacitor	$u_{C\_ac1d}^{(MMCj)}$, $u_{C\_ac1q}^{(MMCj)}$
	2nd voltage component of SM capacitor	$u_{C\_ac2d}^{(MMCj)}$, $u_{C\_ac2q}^{(MMCj)}$
	3rd voltage component of SM capacitor	$u_{C\_ac3x}^{(MMCj)}$, $u_{C\_ac3y}^{(MMCj)}$
	2nd arm current component	$i_{cird}^{(MMCj)}$, $i_{cirq}^{(MMCj)}$
	Measured PCC voltage and current	$u_{sdm}^{(MMCj)}$, $u_{sqm}^{(MMCj)}$, $i_{sdm}^{(MMCj)}$, $i_{sqm}^{(MMCj)}$
	Active power or DC voltage controller	$x_1^{(MMCj)}$ $x_3^{(MMCj)}$
	Reactive power controller	$x_2^{(MMCj)}$ $x_4^{(MMCj)}$
$\boldsymbol{X}_{dcl}$ (l=1,2…N1+N2+1)	Direct voltage	U_{dcl}
	Direct current	I_{dcl}
$\boldsymbol{K}$	Proportional coefficient	k_p
	Integral coefficient	k_i

system can be written as follows:

$$\dot{\boldsymbol{X}}_{n\times 1} = F(\boldsymbol{X}_{\boldsymbol{Idc}}^{\boldsymbol{LCC1}}, \ldots, \boldsymbol{X}_{\boldsymbol{Idc}}^{\boldsymbol{LCCN1}}, \boldsymbol{X}_{\boldsymbol{P}}^{\boldsymbol{MMC1}}, \ldots, \boldsymbol{X}_{\boldsymbol{P}}^{\boldsymbol{MMCN2}}, \boldsymbol{X}_{\boldsymbol{Udc}}^{MMC(N2+1)}, \boldsymbol{X}_{\boldsymbol{dc(N1+N2+1)}}) \tag{6}$$

Then, a 1st-order Taylor expansion is used to linearize (6), and the optimal power flow control parameters in *part. A* are set as the input reference value vector $\boldsymbol{U}_{k\times 1} = [\boldsymbol{U_1}, \boldsymbol{U_2}, \ldots, \boldsymbol{U_k}]^T$. The observed output states are set as the output vector $\boldsymbol{Y}_{m\times 1} = [\boldsymbol{Y_1}, \boldsymbol{Y_2}, \ldots, \boldsymbol{Y_m}]^T$. Finally, based on the state-space matrix method, the complete linearization model of the Hybrid-MTDC system can be expressed as follows:

$$\begin{cases} \Delta\dot{\boldsymbol{X}}_{n\times 1} = \boldsymbol{A}_{n\times n}\Delta\boldsymbol{X}_{n\times 1} + \boldsymbol{B}_{n\times k}\Delta\boldsymbol{U}_{k\times 1} \\ \Delta\boldsymbol{Y}_{m\times 1} = \boldsymbol{C}_{m\times n}\Delta\boldsymbol{X}_{n\times 1} \end{cases} \tag{7}$$

where $\boldsymbol{A}_{n\times n}$ represents the state matrix; $\boldsymbol{B}_{n\times k}$ represents the input matrix; and $\boldsymbol{C}_{m\times n}$ represents the output matrix. Since the model of the Hybrid-MTDC system does not have the states directly formed by the reference value, there is no direct transfer matrix $\boldsymbol{D}$. When the system is running in a steady state, $\boldsymbol{A}_{n\times n}$ is determined by the control parameters $\boldsymbol{K} = [\boldsymbol{k}_{pdc}^{LCC1}, \boldsymbol{k}_{idc}^{LCC1}, \ldots, \boldsymbol{k}_{p1}^{MMC(N2+1)}, \boldsymbol{k}_{i1}^{MMC(N2+1)}]^T$ of the PI controllers in the Hybrid-MTDC system. Therefore, according to the *Lyapunov indirect method*, the stability of

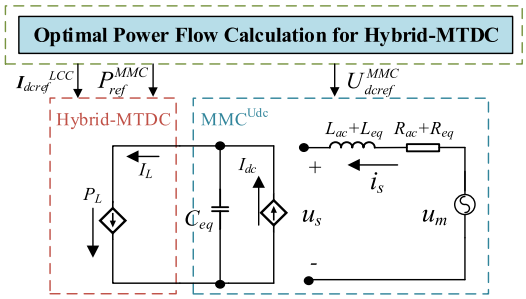

FIGURE 3. Simplified model of an MMC station controlling the DC voltage.

the control parameters can be judged by

$$\begin{cases} Re(\boldsymbol{\lambda}) < 0 \Leftrightarrow \textit{the system is stable} \\ Re(\boldsymbol{\lambda}) \geq 0 \Leftrightarrow \textit{the system is unstable} \\ \textit{where } |\boldsymbol{\lambda E} - \boldsymbol{A}_{n\times n}| = 0 \end{cases} \tag{8}$$

where $\boldsymbol{E}$ is a unit matrix; $\boldsymbol{\lambda}$ is the eigenvalue vector of the state matrix.

Hence, taking different combinations of control parameters $\boldsymbol{K} = [\boldsymbol{k}_{pdc}^{LCC1}, \boldsymbol{k}_{idc}^{LCC1}, \ldots, \boldsymbol{k}_{p1}^{MMC(N2+1)}, \boldsymbol{k}_{i1}^{MMC(N2+1)}]^T$ and using (6)-(8) for fast traversal calculations, the stability range of the control parameters under small-signal disturbances on the converter station layer can be obtained.

C. ADDITIONAL STABILITY CRITERION DEDUCTION

The MMC station, which control the DC voltage of Hybrid-MTDC systems, is the most important part of the system for maintaining its operation [6]. However, the system is linearized by 1st-order Taylor expansion around the equilibrium point in the previous section, but no information is provided about the range from the equilibrium point within which the linearization would remain valid [23]. In engineering, more stringent and specific stability and performance requirements for DC voltage controllers are essential to guarantee reliable operation. Hence, it is necessary to examine the global stability of the DC voltage of the system.

Thus, the *mixed-potential theory*, a form of the Lyapunov function construction method [24], is adopted to deduce the large signal stability criterion for the DC voltage controller of the Hybrid-MTDC system. When the other control parameters satisfy the small-signal stability regions in (8), the Hybrid-MTDC can be simplified as shown in Fig. 3. For readability, the superscript MMC(N2+1) of the variables in the DC voltage control station is omitted in this section. The physical meanings of the variables are also listed in Tab. 1.

Because u_{sq} is controlled near zero by the phase-locked loop (PLL) during normal operation, substituting $u_{sq} = 0$ into (9), the output DC current of the station can be determined as follows:

$$P = \frac{3}{2}(u_{sd}i_{sd} + u_{sq}i_{sq}) = U_{dc} \cdot I_{dc} \tag{9}$$

$$I_{dc} = \frac{3u_{sd}i_{sd}}{2U_{dc}} \tag{10}$$

Based on the *mixed-potential theory* [23], [24], for the simplified model of an MMC station controlling the DC

voltage, the current potential of the non-storage electrical elements can be defined as follows:

$$\begin{aligned}\int\sum_{\mu>r+s} v_\mu di_\mu &= \int_0^{i_{sd}} (u_{md}-u_{sd})di_{sd} - \int_0^{i_{sd}} (R_{ac}+R_{eq})i_{sd}di_{sd} \\ &\quad + \int_0^{I_{dc}} U_{dc}dI_{dc} - \int_0^{I_L} U_{dc}dI_L \\ &= (u_{md}-u_{sd})i_{sd} - \frac{1}{2}(R_{ac}+R_{eq})i_{sd}^2 + U_{dc}I_{dc} \\ &\quad - \int_0^{U_{dc}} I_{dc}dU_{dc} - \frac{1}{2}P_L \end{aligned} \tag{11}$$

where $L_{eq} = L_T + L_{arm}/2$ is the AC system equivalent impedance; $R_{eq} = R_T + R_{arm}/2$ is the AC system equivalent resistance; and P_L is the output active power of the MMC station; u_m is the rated voltage of the AC system

The energy of the equivalent capacitor on the MMC station controlling the DC voltage can be defined as follows:

$$\sum_{\delta=r+1}^{r+s} i_\delta v_\delta = -(I_{dc}-I_L)U_{dc} = -U_{dc}I_{dc} + P_L \tag{12}$$

where r and s are the branches of the current and voltage variables.

By constructing the energy contained in the inductive, capacitive and non-storage elements of the nonlinear circuit, the Lyapunov function, which can be used to describe the energy state of the simplified model, is obtained in unified form as follows:

$$\begin{aligned} &P(i,v) \\ &= -A(i) + B(v) + (i, \gamma v - \alpha) \\ &= \int \sum_{\mu>r+s} v_\mu di_\mu + \sum_{\delta=r+1}^{r+s} i_\delta v_\delta \\ &= (u_{md}-u_{sd})i_{sd} - \frac{(R_{eq}+R_{ac})i_{sd}^2}{2} - \int_0^{U_{dc}} I_{dc}dU_{dc} + \frac{1}{2}P_L \end{aligned} \tag{13}$$

where $A(i)$ is the current potential function of the non-energy storage components in the nonlinear circuit; $B(v)$ is the voltage potential function of the non-energy storage component in the circuit; γ is a circuit structure-related constant matrix; α is a constant vector; and $(i, \gamma v - \alpha)$ is the energy of non-energy storage elements and capacitors.

From Fig. 2, the mathematical model of the outer loop in DC voltage controller can be deduced as follows:

$$\begin{cases} C_{eq}\dfrac{dU_{dc}}{dt} = \dfrac{3}{2U_{dc}}(u_{sd}i_{sd}+u_{sq}i_{sq}) - \dfrac{P_L}{U_{dc}} \\ i_{sdref} = k_{p1}(U_{dcref}-U_{dc}) + k_{i1}\int (U_{dcref}-U_{dc})dt \\ u_{sd} = u_{md} - R_{ac}i_{sd} + \dfrac{L_{ac}}{L_{eq}}R_{eq}i_{sd} \\ \quad + \dfrac{L_{eq}+L_{ac}}{L_{eq}}(\omega L i_{sq} - k_{p3}(i_{sdref}-i_{sd}) - k_{p4}\int (i_{sdref}-i_{sd})dt \end{cases} \tag{14}$$

Based on the 3-rd theorem of the mixed-potential theory [23], [24], the stability criterion can be defined as below:

$$\begin{cases} if\ \mu_1+\mu_2 > 0\ and\ P^*(i,v) \to \infty\ as\ |i|+|v| \to \infty \\ where\ P^*(i,v) = \left(\dfrac{\mu_1+\mu_2}{2}\right)P(i,v) + \dfrac{1}{2}(P_i, L^{-1}P_i) \\ \qquad + \dfrac{1}{2}(P_v, C^{-1}P_v) \\ \mu_1 = eig(L^{-1/2}A_{ii}(i)L^{-1/2}),\quad \mu_2 = eig(C^{-1/2}B_{ii}(i)C^{-1/2}) \\ P_i = \dfrac{\partial P(i,v)}{di},\quad P_i = \dfrac{\partial P(i,v)}{di} \\ A_{ii}(i) = \dfrac{\partial^2 A(i)}{di^2},\quad B_{vv}(v) = \dfrac{\partial^2 B(v)}{dv^2} \end{cases} \tag{15}$$

Here, *eig(.)* means the eigenvalues of the matric.

Substituting (9)-(14) into (15), the additional stability criterion can be written as follows:

$$\begin{aligned} &\frac{R_{eq}+R_{ac}}{L_{ac}+L_{eq}} \\ &\quad - \frac{3Ni_{sdref}[(\frac{L_{ac}+L_{eq}}{L_{eq}})k_{p1}k_{p3}U_{dc} - u_{sd} + (R_{eq}+R_{ac})i_{sdref})}{12C_mU_{dc}^2} \\ &\quad - \frac{NP_L}{6C_mU_{dc}^2} > 0 \end{aligned} \tag{16}$$

where $C_{eq} = 6C_m/N$ and N is the number of the SMs. At the same time, the system should also operate in compliance with the power balance, i.e.,

$$P_L \le \frac{3}{2}[u_{sd}i_{sd} - (R_{ac}+R_{eq})i_{sd}^2] \tag{17}$$

Since the Lyapunov function does not use linearization, it can substitute the accurate abrupt value of the AC or DC side to the criteria (16) and (17), to obtain the additional constraint of the control parameters of the DC voltage controller under any large disturbance.

D. PARAMETRIC DYNAMIC PERFORMANCE ANALYSIS

Within the design-oriented boundaries of controllers, a parametric dynamic performance analysis method is needed to optimize the control parameters of PI controllers on the station layer. Using the Laplace transform, the matrix (7) can be transformed into a transfer function matrix as follows:

$$\begin{cases} \boldsymbol{G}(s) = \dfrac{\Delta \boldsymbol{Y}_{m\times 1}(s)}{\Delta \boldsymbol{U}_{k\times 1}(s)} = \begin{pmatrix} G_{11}(s) & G_{12}(s) & \cdots & G_{1k}(s) \\ G_{21}(s) & G_{22}(s) & \cdots & G_{2k}(s) \\ \vdots & \vdots & \ddots & \vdots \\ G_{m1}(s) & G_{m2}(s) & \cdots & G_{mk}(s) \end{pmatrix}_{m\times k} \\ \Delta \boldsymbol{Y}_{m\times 1}(s) = \boldsymbol{C}_{m\times n}(s\boldsymbol{I}_{n\times n} - \boldsymbol{A}_{n\times n})^{-1}\boldsymbol{B}_{n\times k}\Delta \boldsymbol{U}_{k\times 1}(s) \end{cases} \tag{18}$$

Without loss of generality, the transform function can be written as below:

$$G_{mk}(s) = \frac{b_0 s^q + b_1 s^{q-1} + \cdots + b_{q-1}s + b_q}{a_0 s^r + a_1 s^{r-1} + \cdots + a_{r-1}s + a_r},\ q \le r \tag{19}$$

TABLE 2. Parameters of the Hybrid 3-Terminal HVDC study system.

LCC1 System	Parameters
AC system line voltage	525 kV
AC system frequency	50 Hz
L_{ac}, L_t, R_{ac}	0.002 H, 0.0001H 0
AC filter resistance	R_{r1}=83.32, R_{r2}=261.87, R_{r3}=29.76Ω
AC filter inductance	L_{r1}=0.0136, L_{r2}=0.1364 H
AC filter capacitance	C_{r1}=3.34, C_{r2}=6.69 μF C_{r3}=6.69, C_{r4}=74.28 μF
Current measure time T_{is}	1.2 ms
MMC1	Parameters
AC system line voltage	525 kV
AC system frequency	50 Hz
L_{ac}, R_{ac}	0.001 H, 0
L_t, R_t	0.01 H, 0
L_{arm}, R_{arm}	0.05 H, 0
Submodule capacitance C_m	0.015 F
Voltage measure time T_{us}	0.5 ms
Current measure time T_{is}	0.5 ms
MMC2	Parameters
AC system line voltage	525 kV
AC system frequency	50 Hz
L_{ac}, R_{ac}	0.001 H, 0
L_t, R_t	0.01 H, 0
L_{arm}, R_{arm}	0.05 H, 0
Submodule capacitance C_m	0.015 F
Voltage measure time T_{us}	0.5 ms
Current measure time T_{is}	0.5 ms
DC Link	Parameters
Smoothing reactor of LCC L_{dc}	0.15 H
Resistor (R_0) /km	0.0125 Ω
Inductor (L_0) /km	0.88 mH
Capacitor (C_0) /km	0.013 μF
Reference value/Capacity	Parameters
DC voltage reference value U_B	800 kV
Active power reference value P_B	1000 MW
Rated capacity of stations $S_{LCC}{}^B$, $S_{MMC1}{}^B$, $S_{MMC2}{}^B$	5000, 2000, 3000 MW
Operating DC voltage range of the stations	$95\%<U_{dc}*<105\%$

where a_i and b_j are the coefficients of the molecular and denominator, respectively. Following that, substituting a step response into (19) yields the frequency-domain response model, which can be transformed as a time-domain expression using the Laplace inverse as follows:

$$\Delta Y_m(t) = Laplace^{-1}[\Delta Y_m(s) = G_{mk}(s)/s = \sum_{j=0}^{r} \frac{w_j}{(s-\lambda_j)^m}]$$
$$= \sum_{j=r_2+1}^{r} (-\sqrt{\sigma_j^2+\omega_j^2}) \cdot e^{\sigma_j t} \sin(\omega_j t + \phi_j) + \sum_{j=r_1+1}^{r_2} \frac{1}{(m-1)!} w_{j+m-1} t^{m-1} e^{(\sigma_j + j\omega_j)t} + \sum_{j=0}^{r_1} w_j e^{(\sigma_j+j\omega_j)t} \quad (20)$$

where λ_j is the solution of the eigenvalue equation $\sum_{j=0}^{r} b_j s^j$; w_j is the coefficient of each item after factorization; $\lambda_j = \sigma_j + j\omega_j$; and $\phi_j = \tan^{-1}[\frac{-\sigma_j}{\omega_j}]$.

When each state X of the system is taken as the output variable, from (20), it is obvious that the eigenvalues of the system state matrix $\boldsymbol{A}_{n\times n}$ can be divided into real eigenvalues and complex eigenvalues. The real eigenvalues correspond to a non-oscillatory mode. The positive real part represents the nonperiodic divergence instability, and the negative real part corresponds to the attenuation mode. The larger the absolute value is, the faster the attenuation will be. Complex eigenvalues of conjugate $\lambda_j = \sigma_j + j\omega_j$ correspond to the oscillation mode. The damping ratio $\zeta_k = -\sigma_k/\sqrt{\sigma_k^2+\omega_k^2}$ determines the attenuation speed of the oscillation amplitude. In addition, the higher the damping ratio is, the faster the attenuation will be.

Thus, the evaluation index for the parametric dynamic performance analysis of the system controllers can be established as follows:

$$F = \sum_{k=1}^{j} \gamma_k \left|\sigma_k - \sigma^*\right| + \sum_{k=1}^{i} \beta_k \left|\zeta^* - \zeta_k\right|$$
$$\zeta_k = -\sigma_k/\sqrt{\sigma_k^2+\omega_k^2} \quad (21)$$

where γ_k is the weight of the real eigenvalue, β_k is the weight of the oscillating modal damping ratio; and σ^* and ζ^* are the ideal values. The minimum F means that the corresponding control parameters are with the optimal dynamic performances.

In sum, the specific process of the proposed control parameter design method for Hybrid MTDC systems is depicted in Fig 4.

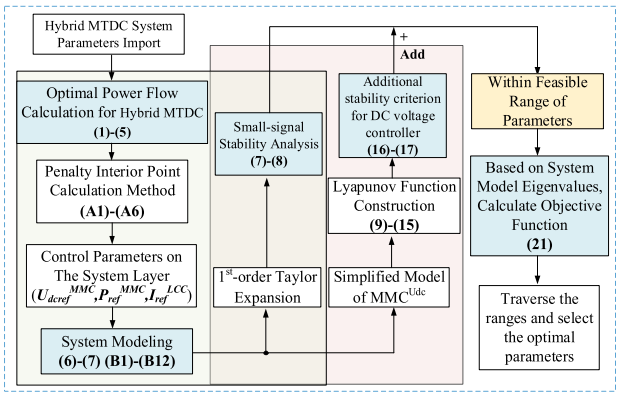

FIGURE 4. Flow chart of the control parameter design method.

III. CASE STUDIES AND ANALYSIS

A. 3-TERMINAL HYBRID HVDC SYSTEM FOR MODELING AND SIMULATION

A hybrid 3-terminal HVDC system is used to validate the correctness of the proposed method, as shown in Fig. 5. The parameters of the study system are referred to as the CIGRE model and the existing projects, as follows:

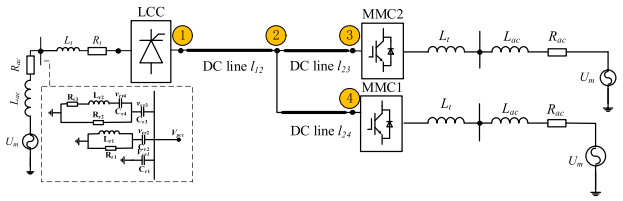

FIGURE 5. Hybrid 3-terminal HVDC system.

TABLE 3. Optimization power flow control parameters.

DC nodes	ω_1=0.5, ω_2=0.5		ω_1=0.2, ω_2=0.8		ω_1=0, ω_2=1	
	U_{dc} (p.u.)	P (p.u.)	U_{dc} (p.u.)	P (p.u.)	U_{dc} (p.u.)	P (p.u.)
1	0.9988	3.9952	0.9989	3.9956	0.9995	3.998
2	0.9819	/	0.9820	/	0.9827	/
3	0.9711	1.9422	0.9710	1.9424	0.9686	2.5086
4	0.9777	1.9554	0.9779	1.9556	0.9797	1.3814
f_1 (loss)	0.0976 p.u.		0.0982 p.u.		0.108 p.u.	
f_2 (ΔU)	0.0066 p.u.		0.0062 p.u.		0.0048 p.u.	

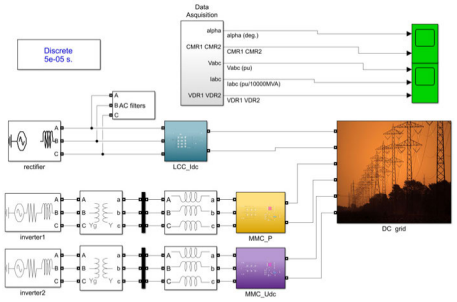

FIGURE 6. Hybrid 3-terminal HVDC simulation system.

B. OPTIMAL POWER FLOW CONTROL CALCULATION

According to the optimal power flow control calculation method in (1)-(5) and (A1)-(A6), the control parameters in the system layer are calculated in MATLAB for different combinations of ω_1 and ω_2. The results are shown in Tab 3.

Choosing $\omega_1 = 0.5$ and $\omega_2 = 0.5$ as an example, the control parameters ($\boldsymbol{I}_{dcref}^{LCC}$, $\boldsymbol{P}_{ref}^{MMC}$, $\boldsymbol{U}_{dcref}^{MMC}$) of each station can be obtain according to Tab 3, and then are set as the reference control values of the stations in the simulation model and the mathematical model, separately. According to the hybrid 3-terminal HVDC system structure, as shown in Fig. 5, a mathematical model with 83 orders can be constructed and linearized in the state-space matrix by (B1)-B(12). To validate the mathematical model for the control parameter design method, this paper establishes a simulation model for the corresponding hybrid 3-terminal HVDC using the detailed electrical model in Simulink, as shown in Fig. 6.

C. MATHEMATICAL MODEL VERIFICATION

The responses of the simulation and the mathematical model after introducing a 26-kV step signal to the reference value U_{dcref}^{MMC} of MMC2, which control the DC voltage of the system, can be seen in Fig. 7.

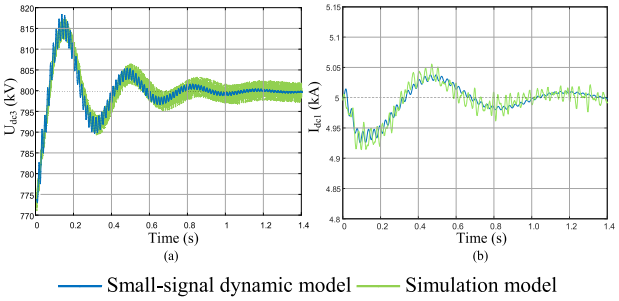

FIGURE 7. Dynamic characteristics of the system when the voltage is stepped. (a) Response of the DC voltage. (b) Response of the DC current.

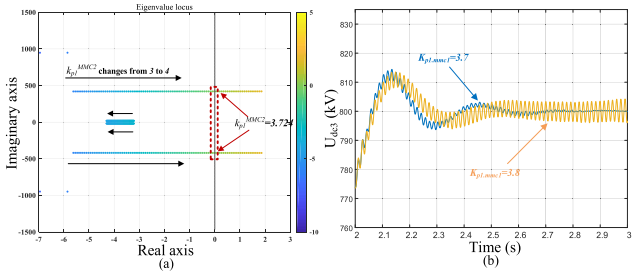

FIGURE 8. Lyapunov indirect method verification. (a) Eigenvalue locus of the system when k_{p1}^{MMC2} changes from 3 to 4. (b) Time-domain response of the system with the critical control parameter values of the left and right sides of the imaginary axis.

Fig. 7 shows the correctness of the model of the hybrid 3-terminal HVDC transmission system. Since the established model does not contain higher-order harmonic characteristics, the fluctuation of the simulated waveform in the figure is larger than the fluctuation of the model output, but the average outputs are basically the same.

D. SMALL-SIGNAL STABILITY ANALYSIS VERIFICA-TION AND FEASIBLE REGIONS

To verify the feasible control parameter regions under the small-signal stability calculated by (7) and (8), the root trajectory of the system is depicted in Fig. 8, when the gain parameter k_{p1}^{MMC2} of MMC2 is gradually increased. The two values of k_{p1}^{MMC2}, with the eigenvalue crossing the imaginary axis, are respectively analysed and compared under a small step signal to the reference value U_{dcref}^{MMC} of MMC2 in the Simulink simulation.

It can be seen from Fig. 8 that the PI control parameters corresponding to the eigenvalues located on the left side of the imaginary axis can restore a gradual stable state, while the PI control parameters corresponding to the right side of the imaginary axis are divergent. Hence, repeated calculation by (6)-(8), the control parameter feasible regions with small-signal stability can be obtained through traversal control parameters, as shown in Fig. 9.

When the control parameters of LCC and MMC1 satisfy the range of Fig. 9(a) and (b), the specific criteria are further added for the DC voltage control station MMC2 in the next part based on engineering requirements.

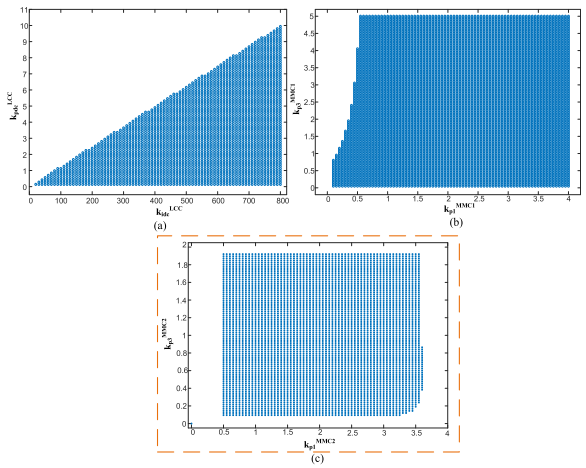

FIGURE 9. Feasible regions under small-signal stability. (a) Control parameter feasible region of the LCC. (b) Control parameter feasible region of MMC1. (c) Control parameter feasible region of MMC2.

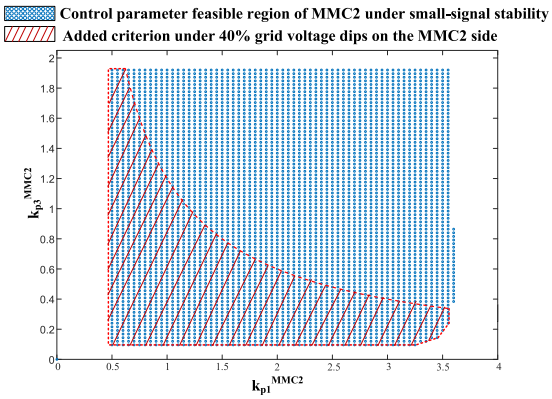

FIGURE 10. Added criterion for the stability under 40% grid voltage dipping.

E. ADDITIONAL STABILITY CRITERION VERIFICATION

To verify the correctness of the additional stability criterion for the U_{dc} controller in the Hybrid-MTDC, a large step dip in the grid voltage occurs in transient simulations to imitate the practical grid faults. For instance, the grid voltage dips 40% on the MMC2 side in the hybrid 3-terminal HVDC transmission system, and the ramping process lasts for 100 ms. Using (9)-(17) to calculate the constraints of these wide-ranging disturbances of the AC system, the responding criterion of the control parameters is plotted in Fig. 10.

Three sets of different control parameters are taken for comparison verification, as shown in TAB 4, and the responses of the simulations are compared with the calculation results.

The simulations are displayed as shown in Fig 11, while the grid voltage U_m^{MMC2} on the MMC2 side dips 40% at 1.5 s.

It can be seen from Fig. 11 that only the system with the PI control parameters within the additional criterion is able to remain stable after the steps. It is proved that the when the disturbance is beyond the linearizable range of the Hybrid MTDC system model, the proposed method can effectively analyse the control parameters to maintain a stable range and supplement the corresponding criteria in engineering.

TABLE 4. Calculation results of 3 sets of control parameters.

No.	k_{p1}^{MMC2}	k_{p3}^{MMC2}	Small-signal stability region	Additional stability constraint
a	3.800	0.48	Not satisfied	Not satisfied
b	3.509	0.48	Satisfied	Not satisfied
c	2.460	0.37	Satisfied	Satisfied

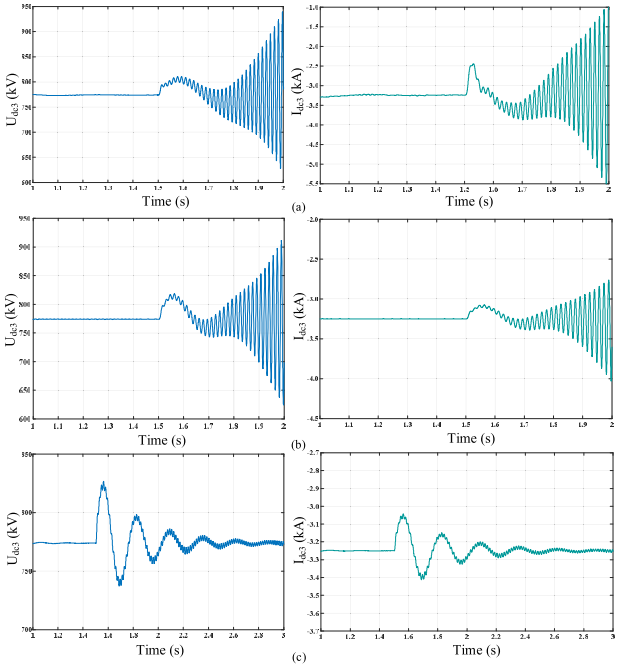

FIGURE 11. Simulations for additional stability. (a) Unstable operation with the grid voltage dip leading to state divergence. (b) Unstable operation with the same dip. (c) Stable operation with the same dip.

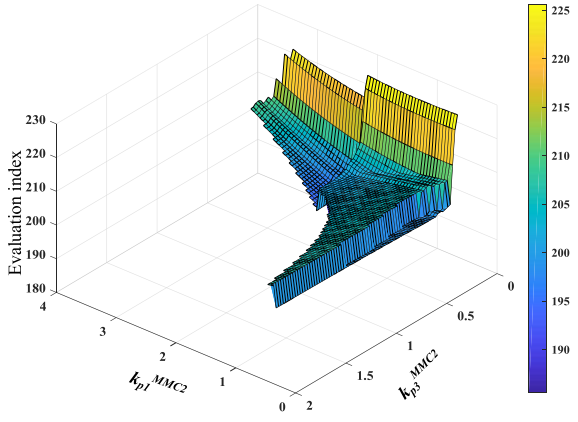

FIGURE 12. The impact of the control performance based on the region in Fig. 10.

F. PARAMETRIC DYNAMIC PERFORMANCE EVALUA-TION INDEX AND OPTIMIZATION

Within the feasible range in Fig. 10, the evaluation index for the parametric dynamic performance can be calculated

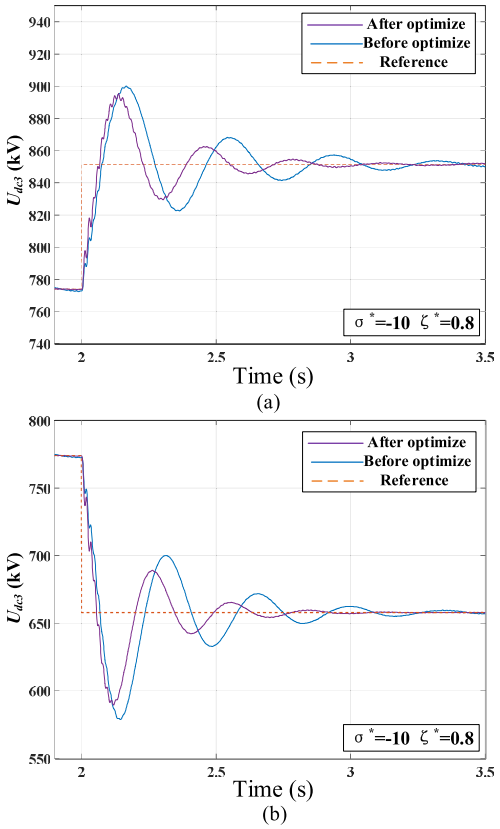

FIGURE 13. The simulation responses of U_{dc3}. (a) The responses of U_{dc3} before and after the parameter +10% step adjustment. (b) The responses of U_{dc3} before and after the parameter −15% step adjustment.

TABLE 5. Single performance indicator comparison.

	10% DC voltage increase		15% DC voltage reduction	
	Overshoot	Adjustment time	Overshoot	Adjustment time
Bef-opt	5.9%	1.00 s	12.0%	0.88 s
Aft-opt	5.2%	0.62 s	10.3%	0.47 s

using (21) through traversal control parameters. Because the proposed evaluation index only needs to calculate the matrix eigenvalues, the calculation is significantly faster than the simulation analysis that requires discrete numerical solutions. Then, taking the U_{dc} controller for instance, 3-dimensional numerical coordinates describing the dynamic performance of the system can be constructed, shown in Fig. 12. The minimum values of the evaluation indices of the parameters are taken as the control parameters after the optimization.

To validate the correctness of the proposed method, the simulations are displayed as follows: 1) When the system is running stably, the reference DC voltage U_{dcref}^{MMC2} is increased by 10% at 2.0 s. The response to this adjustment is shown in Fig. 13(a). 2) The reference DC voltage U_{dcref}^{MMC2} is reduced by 15% at 2.0 s, and the response to this adjustment is shown in Fig. 13(b). Both experiments are carried out with Simulink-based simulations.

From the comparative analysis in Tab. 5, the parameters after optimization (aft-opt) reduce the overshoot and the adjusting time of the responses, thus verifying the effectiveness of the proposed control parameter design method.

IV. CONCLUSION

On the system layer, using the normalization processing method, a system-layer objective function that considers both the minimum network loss and the voltage offset is formed for Hybrid-MTDC systems and solved with the proposed penalty interior point method in this paper. On the converter layer, using the state-space matrix method, a generic small-signal stability range for each control parameter can be obtained by the traversal calculation of the eigenvalues. Then, to identify the additional stable operating region for the DC voltage controller, an additional stability analysis based on the mixed-potential theory is performed and the design-oriented boundaries are generated and added to the feasible region. Finally, within the design-oriented boundaries, a dynamic performance evaluation function is constructed to optimize the control parameters.

From a typical case analysis, utilizing the proposed method, the system can run in the optimal power flow control. Due to the addition of specific stability criteria, the system can maintain stable operation over a large disturbance range. Finally, within the design-oriented boundaries, the dynamic performance of the system control is effectively adjusted to the optimal state based on the proposed dynamic performance evaluation function.

APPENDIX

A. PENALTY INTERIOR POINT METHOD CALCULATION

The optimality condition corresponding to function (5) can be obtained as the Kuhn-Tucker condition:

$$\begin{cases} \boldsymbol{L}_{\boldsymbol{x}}^{'} = \boldsymbol{f}_{\boldsymbol{x}}^{'}(\boldsymbol{x}) - \boldsymbol{h}_{\boldsymbol{x}}^{'}(\boldsymbol{x})y - \boldsymbol{g}_{\boldsymbol{x}}^{'}(\boldsymbol{x})(z+x) \\ \boldsymbol{L}_{\boldsymbol{y}}^{'} = \boldsymbol{h}(\boldsymbol{x}) = 0 \\ \boldsymbol{L}_{\boldsymbol{z}}^{'} = \boldsymbol{g}(\boldsymbol{x}) - \boldsymbol{l} - \boldsymbol{g}_{\boldsymbol{l}} = 0 \\ \boldsymbol{L}_{\boldsymbol{w}}^{'} = \boldsymbol{g}(\boldsymbol{x}) + \boldsymbol{u} - \boldsymbol{g}_{\boldsymbol{h}}(\boldsymbol{x}) = 0 \\ \boldsymbol{L}_{\boldsymbol{l}}^{'} = \boldsymbol{Z} - \mu \boldsymbol{U}^{-1}\boldsymbol{I} = 0 \\ \boldsymbol{L}_{\boldsymbol{u}}^{'} = -\boldsymbol{W} - \mu \boldsymbol{L}^{-1}\boldsymbol{I} = 0 \end{cases} \tag{A1}$$

where $\boldsymbol{h}_{\boldsymbol{x}}^{'}(\boldsymbol{x})$ and $\boldsymbol{g}_{\boldsymbol{x}}^{'}(\boldsymbol{x})$ are the Jacobian matrix; $\boldsymbol{L} = \mathrm{diag}\{l\}$; $\boldsymbol{U} = \mathrm{diag}\{u\}$; $\boldsymbol{Z} = \mathrm{diag}\{z\}$; $\boldsymbol{W} = \mathrm{diag}\{w\}$; $\boldsymbol{I} = [1,\ldots\ldots,1]$.

The above equation is solved using the Newton method. In order to reduce the dimension of the modified equation, the approximate correction equation is given as follows:

$$\begin{bmatrix} \boldsymbol{H} & \boldsymbol{h}_{\boldsymbol{x}}^{'}(\boldsymbol{x}) \\ [\boldsymbol{h}_{\boldsymbol{x}}^{'}(\boldsymbol{x})]^{T} & 0 \end{bmatrix} \begin{bmatrix} \Delta \boldsymbol{x} \\ \Delta \boldsymbol{y} \end{bmatrix} = \begin{bmatrix} \boldsymbol{P} \\ -\boldsymbol{L}_{\boldsymbol{y}}^{'} \end{bmatrix} \tag{A2}$$

$$\begin{bmatrix} \boldsymbol{I} & \boldsymbol{L}^{-1}\boldsymbol{Z} \\ 0 & \boldsymbol{I} \end{bmatrix} \begin{bmatrix} \Delta \boldsymbol{z} \\ \Delta \boldsymbol{l} \end{bmatrix} = \begin{bmatrix} -\boldsymbol{L}^{-1}\boldsymbol{L}_{\boldsymbol{l}\mu}^{''} \\ \boldsymbol{L}_{\boldsymbol{z}}^{'} + [\boldsymbol{g}_{\boldsymbol{x}}^{'}(\boldsymbol{x})]^{T}\Delta \boldsymbol{x} \end{bmatrix} \tag{A3}$$

$$\begin{bmatrix} \boldsymbol{I} & \boldsymbol{U}^{-1}\boldsymbol{W} \\ 0 & \boldsymbol{I} \end{bmatrix} \begin{bmatrix} \Delta \boldsymbol{w} \\ \Delta \boldsymbol{u} \end{bmatrix} = \begin{bmatrix} -\boldsymbol{U}^{-1}\boldsymbol{L}_{\boldsymbol{u}\mu}^{''} \\ \boldsymbol{L}_{\boldsymbol{w}}^{'} + \boldsymbol{g}_{\boldsymbol{x}}^{'}(\boldsymbol{x})\Delta \boldsymbol{x} \end{bmatrix} \tag{A4}$$

where

$$\boldsymbol{H} = -\boldsymbol{f}''_{\boldsymbol{xx}}(\boldsymbol{x}) - \boldsymbol{h}''_{\boldsymbol{xx}}(\boldsymbol{x})y - \boldsymbol{g}''_{\boldsymbol{xx}}(\boldsymbol{x})(z+x) - \boldsymbol{g}'_{\boldsymbol{x}}(\boldsymbol{x})[\boldsymbol{L}^{-1} \times \boldsymbol{Z} - \boldsymbol{U}^{-1}\boldsymbol{W}][\boldsymbol{g}'_{\boldsymbol{x}}(\boldsymbol{x})]^T$$

$$\boldsymbol{P} = \boldsymbol{L}'_{\boldsymbol{x}} + \boldsymbol{g}'_{\boldsymbol{x}}(\boldsymbol{x}) \cdot [\boldsymbol{L}^{-1}(\boldsymbol{L}''_{\boldsymbol{l\mu}} + \boldsymbol{Z}\boldsymbol{L}''_{\boldsymbol{z}}) + \boldsymbol{U}^{-1}(\boldsymbol{L}''_{\boldsymbol{u\mu}} + \boldsymbol{W}\boldsymbol{L}'_{\boldsymbol{w}})].$$

By solving (A2)–(A4), the (k+1)-th iteration variables can be obtained as:

$$x_{j,k+1} = x_{j,k} + \Delta x_{j,k}, \quad j = 1, \ldots, N1 + N2 + 1 \tag{A5}$$

When (A6) is satisfied, the iteration terminates:

$$\frac{\left|x_{j,k+1} - x_{j,k}\right|}{x_{j,k}} \le \xi \tag{A6}$$

B. SYSTEM MODELING

The LCC equivalent model can be divided into connected AC system and equivalent converter. The AC system can be described as

$$\begin{cases} di_{sd}/dt = (-v_{\mathrm{pccd}} - R_{ac}i_{\mathrm{sd}} + U_m \sin(-x_{PLL}))/L_{ac} - \omega \cdot i_{\mathrm{sq}} \\ di_{sq}/dt = (-v_{\mathrm{pccq}} - R_{ac}i_{\mathrm{sq}} + U_m \cos(-x_{PLL}))/L_{ac} + \omega \cdot i_{\mathrm{sd}} \end{cases} \tag{B1}$$

where R_{ac} and L_{ac} are the equivalent impedances of the AC system. U_m is the equivalent voltage amplitude of the AC system.

Also, if the AC filters are included in the LCC side, it can be deduced as

$$\begin{cases} dv_{pccd}/dt = -\omega \cdot v_{\mathrm{pccq}} + e_1(v_{\mathrm{Cr2d}} - v_{\mathrm{pccd}}) + e_2(v_{\mathrm{Cr3d}} - v_{\mathrm{pccd}}) + (i_{\mathrm{sd}} - i_{\mathrm{Lr1d}} - i_{\mathrm{Lr2d}} - i_{\mathrm{cd}})/C_{r1} \\ dv_{pccq}/dt = \omega \cdot v_{\mathrm{pccd}} + e_1(v_{\mathrm{Cr2q}} - v_{\mathrm{pccq}}) + e_2(v_{\mathrm{Cr3q}} + v_{\mathrm{pccq}}) + (i_{\mathrm{sq}} - i_{\mathrm{Lr1q}} - i_{\mathrm{Lr2q}} - i_{\mathrm{cq}})/C_{r1} \\ dv_{Cr2d}/dt = e_3(v_{\mathrm{pccd}} - v_{\mathrm{Cr2d}}) - \omega \cdot v_{\mathrm{Cr2q}} + i_{\mathrm{Lr1d}}/C_{r2} \\ dv_{Cr2q}/dt = e_3(v_{\mathrm{pccq}} - v_{\mathrm{Cr2q}}) + \omega \cdot v_{\mathrm{Cr2d}} + i_{\mathrm{Lr1q}}/C_{r2} \\ di_{Lr1d}/dt = (v_{\mathrm{pccd}} - v_{\mathrm{Cr2d}})/L_{r1} - \omega \cdot i_{\mathrm{Lr1q}} \\ di_{Lr1q}/dt = (v_{\mathrm{pccq}} - v_{\mathrm{Cr2q}})/L_{r1} + \omega \cdot i_{\mathrm{Lr1d}} \\ dv_{Cr3d}/dt = e_4(v_{\mathrm{pccd}} - v_{\mathrm{Cr3d}}) - \omega \cdot v_{\mathrm{Cr3q}} + i_{\mathrm{Lr2d}}/C_{r3} \\ dv_{Cr3q}/dt = e_4(v_{\mathrm{pccq}} - v_{\mathrm{Cr3q}}) + \omega \cdot v_{\mathrm{Cr3d}} + i_{\mathrm{Lr2q}}/C_{r3} \\ dv_{Cr4d}/dt = -\omega \cdot v_{\mathrm{Cr4q}} + i_{\mathrm{Lr2d}}/C_{r4} \\ dv_{Cr4q}/dt = \omega \cdot v_{\mathrm{Cr4d}} + i_{\mathrm{Lr2q}}/C_{r4} \\ di_{Lr2d}/dt = (v_{\mathrm{pccd}} - v_{\mathrm{Cr3d}} - v_{\mathrm{Cr4d}} - R_{r3}i_{\mathrm{Lr2d}})/L_{r2} - \omega \cdot i_{\mathrm{Lr2q}} \\ di_{Lr2q}/dt = (v_{\mathrm{pccq}} - v_{\mathrm{Cr3q}} - v_{\mathrm{Cr4q}} - R_{r3}i_{\mathrm{Lr2q}})/L_{r2} + \omega \cdot i_{\mathrm{Lr2d}} \end{cases} \tag{B2}$$

The equivalent converter of LCC can be deduced as

$$\begin{cases} i_{\mathrm{cd}} = 2I_{\mathrm{dcr}}k_T \dfrac{2\sqrt{3}}{\pi} \dfrac{\sin(\mu/2)}{\mu/2} \left(\dfrac{\cos\alpha + \cos(\alpha + \mu/2)}{2}\right) \\ i_{\mathrm{cq}} = 2I_{\mathrm{dcr}}k_T \dfrac{2\sqrt{3}}{\pi} \dfrac{\sin(\mu/2)}{\mu/2} \sin\left(\cos^{-1}\left(\dfrac{\cos\alpha + \cos(\alpha + \mu/2)}{2}\right)\right) \end{cases} \tag{B3}$$

where $\mu = \arccos(\cos\alpha - \frac{\sqrt{2}\,X_T I_{\mathrm{dcr}}}{v_{\mathrm{pcc}}k_T}) - \alpha$; α is the delay angle of thyristor conduction.

The controllers of the LCC stations, as shown in Fig. 2 can be described as

$$\begin{cases} \pi - \alpha = k_{pdc}(I^{LCC}_{dcref} - I_{dcm}) - k_{idc}\int (I^{LCC}_{dcref} - I_{dcm})dt \\ U_{dc} = \dfrac{3\sqrt{2}}{\pi} nEK\cos\alpha - \dfrac{3 \cdot 2\pi f L_t}{\pi} nI_{dc} \\ dx_{PLL}/dt = -k_{pPLL}u_{sq} - k_{iPLL}\int u_{sq}dt \\ \omega = \omega_0 + dx_{PLL}/dt \end{cases} \tag{B4}$$

where E is the equivalent voltage amplitude of the AC system; K is the ratio of converter transformer; n is the number of six-phase pulsating converters.

The MMC equivalent model also can be divided into connected AC system and equivalent model of converter. The description of AC system is the same as the LCC side. And the equivalent model of converter primarily consists of the SM capacity, which can be described as

$$du_{C\_dc}/dt = \frac{1}{6C_m} \cdot I_{dc} + \frac{u_{sq}i_{sq}}{4C_mU_{dc}} + \frac{u_{sd}i_{sd}}{4C_mU_{dc}} + \frac{u_{cirq}i_{cirq}}{2C_mU_{dc}} + \frac{u_{cird}i_{cird}}{2C_mU_{dc}} \tag{B5}$$

where

$$\begin{cases} du_{C\_ac1d}/dt = -\omega u_{C\_ac1q} - \dfrac{1}{4C_m}i_{sd} - \dfrac{I_{dc}u_{sd}}{3C_mU_{dc}} - \dfrac{u_{sq}i_{cirq}}{2C_mU_{dc}} - \dfrac{u_{sd}i_{cird}}{2C_mU_{dc}} - \dfrac{u_{cirq}i_{sq}}{4C_mU_{dc}} - \dfrac{u_{cird}i_{sd}}{4C_mU_{dc}} \\ du_{C\_ac1q}/dt = \omega u_{C\_ac1d} - \dfrac{1}{4C_m}i_{sq} - \dfrac{I_{dc}u_{sq}}{3C_mU_{dc}} - \dfrac{u_{sd}i_{cirq}}{2C_mU_{dc}} - \dfrac{u_{sq}i_{cird}}{2C_mU_{dc}} - \dfrac{u_{cirq}i_{sd}}{4C_mU_{dc}} - \dfrac{u_{cird}i_{sq}}{4C_mU_{dc}} \end{cases} \tag{B6}$$

$$\begin{cases} du_{C\_ac2d}/dt = -\omega u_{C\_ac2q} + \dfrac{1}{2C_m}i_{cird} + \dfrac{I_{dc}u_{cird}}{3C_mU_{dc}} - \dfrac{u_{sq}i_{sq}}{4C_mU_{dc}} + \dfrac{u_{sd}i_{sd}}{4C_mU_{dc}} \\ du_{C\_ac2q}/dt = \omega u_{C\_ac2d} + \dfrac{1}{2C_m}i_{cirq} + \dfrac{I_{dc}u_{cirq}}{3C_mU_{dc}} + \dfrac{u_{sd}i_{sq}}{4C_mU_{dc}} + \dfrac{u_{sq}i_{sd}}{4C_mU_{dc}} \end{cases} \tag{B7}$$

$$\begin{cases} du_{C\_ac3x}/dt = 3\omega u_{C\_ac3y} - \dfrac{i_{cirq}u_{sd}}{2C_mU_{dc}} - \dfrac{u_{sq}i_{cird}}{2C_mU_{dc}} - \dfrac{u_{cird}i_{sq}}{4C_mU_{dc}} - \dfrac{u_{cirq}i_{sd}}{4C_mU_{dc}} \\ du_{C\_ac3y}/dt = -3\omega u_{C\_ac3x} - \dfrac{i_{cirq}u_{sq}}{2C_mU_{dc}} - \dfrac{u_{sd}i_{cird}}{2C_mU_{dc}} - \dfrac{u_{cirq}i_{sq}}{4C_mU_{dc}} - \dfrac{u_{cird}i_{sd}}{4C_mU_{dc}} \end{cases} \tag{B8}$$

And the differential equations of circulating currents are

$$\begin{cases} di_{cird}/dt = -2\omega i_{cirq} - \dfrac{Nu_{C\_ac2d}}{2L_{arm}} - \dfrac{Nu_{C\_dc}i_{cird}}{U_{dc}L_{arm}} - \dfrac{R_{arm}}{L_{arm}}i_{cird} \\ \qquad +N\dfrac{u_{C\_ac1d}u_{sd} - u_{sq}u_{C\_ac1q}}{2U_{dc}L_{arm}} \\ \qquad +N\dfrac{u_{C\_ac3x}u_{sq} - u_{sd}u_{C\_ac3y}}{2U_{dc}L_{arm}} \\ di_{cirq}/dt = 2\omega i_{cird} - \dfrac{Nu_{C\_ac2q}}{2L_{arm}} - \dfrac{Nu_{C\_dc}i_{cirq}}{U_{dc}L_{arm}} - \dfrac{R_{arm}}{L_{arm}}i_{cirq} \\ \qquad +N\dfrac{u_{C\_ac1q}u_{sd} - u_{sq}u_{C\_ac1d}}{2U_{dc}L_{arm}} \\ \qquad +N\dfrac{u_{C\_ac3x}u_{sq} - u_{sd}u_{C\_ac3y}}{2U_{dc}L_{arm}} \end{cases} \tag{B9}$$

where C_m is the capacitance of SM; N is the number of SMs; $L_{eq} = L_T + L_{arm}/2$ is the AC system equivalent impedance; $R_{eq} = R_T + R_{arm}/2$ is the AC system equivalent resistance.

Finally, the double closed loop vector controllers of the MMC stations can be described as

$$\begin{cases} x_1 = \int (P_{ref}^{MMC} - \dfrac{3}{2}u_{sd}i_{sd} - \dfrac{3}{2}u_{sq}i_{sq})dt \ or \int (U_{dcref}^{MMC} - U_{dcm})dt \\ x_2 = \int (Q_{ref} - \dfrac{3}{2}u_{sd}i_{sq} + \dfrac{3}{2}u_{sq}i_{sd})dt \\ i_{sdref} = k_{p1}(P_{ref} - \dfrac{3}{2}u_{sd}i_{sd} - \dfrac{3}{2}u_{sq}i_{sq}) + k_{i1}x_1 \ or \\ \qquad k_{p1}(U_{dcref}^{MMC} - U_{dcm}) + k_{i1}x_1 \\ i_{sqref} = k_{p2}(Q_{ref} - \dfrac{3}{2}u_{sd}i_{sq} + \dfrac{3}{2}u_{sq}i_{sd}) + k_{i1}x_2 \\ x_3 = \int (i_{sdref} - i_{sd})dt \\ x_4 = \int (i_{sqref} - i_{sq})dt \\ u_{cdref} = u_{sdm} - \omega L_{eq}i_{sq} - k_{i3}x_3 - k_{p3}(i_{sdref} - i_{sdm}) \\ u_{cqref} = u_{sqm} + \omega L_{eq}i_{sd} - k_{i4}x_4 - k_{p4}(i_{sqref} - i_{sqm}) \\ du_{sdm}/dt = (u_{sd} - u_{sdm})/T_{usd} \\ du_{sqm}/dt = (u_{sq} - u_{sqm})/T_{usq} \\ di_{sdm}/dt = (i_{sd} - i_{sdm})/T_{isd} \\ di_{sqm}/dt = (i_{sq} - i_{sqm})/T_{isq} \end{cases} \tag{B10}$$

where $T_{usd}, T_{usq}, T_{isd}, T_{isq}$ are the time of measurement.

The circulation suppression controller is expressed in d-q coordinates as

$$\begin{cases} u_{cird} = -2\omega L_{arm}i_{cird} - k_{icir}\int (i_{cirdref} - i_{cird})dt \\ \qquad -k_{pcir}(i_{cirdref} - i_{cird}) \\ u_{cirq} = 2\omega L_{arm}i_{cirq} - k_{icir}\int (i_{cirqref} - i_{cirq})dt \\ \qquad -k_{pcir}(i_{cirqref} - i_{cirq}) \end{cases} \tag{B11}$$

The DC line is an equivalent circuit of π type, shown in Fig. 14, and the current on a DC line can be represented as

$$L_d\frac{dI_{dci}}{dt} = U_{dci} - U_{dcj} - R_dI_{dci} \tag{B12}$$

where R_d and L_d are the equivalent resistance and inductance of the DC line between node i and j; I_{dci} represents the DC current.

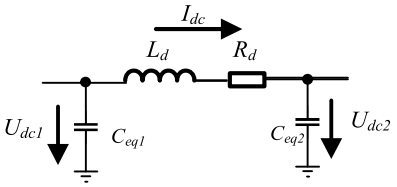

FIGURE 14. Equivalent circuit of DC lines.

REFERENCES

[1] Y. Ma, H. Li, G. Wang, and J. Wu, "Fault analysis and traveling-wave-based protection scheme for double-circuit LCC-HVDC transmission lines with shared towers," *IEEE Trans. Power Del.*, vol. 33, no. 3, pp. 1479–1488, Jun. 2018.

[2] L. Yuansheng, W. Gang, and L. Haifeng, "Time-domain fault-location method on HVDC transmission lines under unsynchronized two-end measurement and uncertain line parameters," *IEEE Trans. Power Del.*, vol. 30, no. 3, pp. 1031–1038, Jun. 2015.

[3] L. Wang, J. Xu, G. Wang, and Z. Zhang, "Lifetime estimation of IGBT modules for MMC-HVDC application," *Microelectron. Rel.*, vol. 82, pp. 90–99, Mar. 2018.

[4] J. Xu, L. Wang, Y. Li, Z. Zhang, G. Wang, and C. Hong, "A unified MMC reliability evaluation based on physics-of-failure and SM lifetime correlation," *Int. J. Elect. Power Energy Syst.*, vol. 106, pp. 158–168, Mar. 2019.

[5] Z. Zhao and M. Iravani, "Application of GTO voltage source inverter in a hybrid HVDC link," *IEEE Trans. Power Del.*, vol. 9, no. 1, pp. 369–377, Jan. 1994.

[6] M. Li, Z. Guo, D. Cai, and G. Wang, "Operating characteristic analysis of multi-terminal hybrid HVDC transmission system with different control strategies," in *Proc. Int. Conf. Power Syst. Technol. (POWERCON)*, Guangzhou, China, 2018, pp. 2616–2621, doi: 10.1109/POWERCON.2018.8602314.

[7] C. Li, P. Zhan, J. Wen, M. Yao, N. Li, and W.-J. Lee, "Offshore wind farm integration and frequency support control utilizing hybrid multi-terminal HVDC transmission," *IEEE Trans. Ind. Appl.*, vol. 50, no. 4, pp. 2788–2797, Jul./Aug. 2014.

[8] J. Qi, V. K. Sood, and V. Ramachandran, "Incremental fuzzy PI control of a HVDC plant," in *Proc. IEEE Conf. Control Appl. (CCA)*, Toronto, ON, Canada, Sep. 2005, pp. 1305–1310.

[9] S. Filizadeh, A. M. Gole, D. A. Woodford, and G. D. Irwin, "An optimization-enabled electromagnetic transient simulation-based methodology for HVDC controller design," *IEEE Trans. Power Del.*, vol. 22, no. 4, pp. 2559–2566, Oct. 2007.

[10] D. Jovcic, N. Pahalawaththa, and M. Zavahir, "Analytical modelling of HVDC-HVAC systems," *IEEE Trans. Power Del.*, vol. 14, no. 2, pp. 506–511, Apr. 1999.

[11] C. Osauskas and A. Wood, "Small-signal dynamic modeling of HVDC systems," *IEEE Trans. Power Del.*, vol. 18, no. 1, pp. 220–225, Jan. 2003.

[12] J. Xu, A. M. Gole, and C. Zhao, "The use of averaged-value model of modular multilevel converter in DC grid," *IEEE Trans. Power Del.*, vol. 30, no. 2, pp. 519–528, Apr. 2015.

[13] Y. Li, G. Tang, J. Ge, Z. He, H. Pang, J. Yang, and Y. Wu, "Modeling and damping control of modular multilevel converter based DC grid," *IEEE Trans. Power Syst.*, vol. 33, no. 1, pp. 723–735, Jan. 2018.

[14] T. Li, A. M. Gole, and C. Zhao, "Harmonic instability in MMC-HVDC converters resulting from internal dynamics," *IEEE Trans. Power Del.*, vol. 31, no. 4, pp. 1738–1747, Aug. 2016.

[15] C. Guo, Z. Yin, C. Zhao, and R. Iravani, "Small-signal dynamics of hybrid LCC-VSC HVDC systems," *Int. J. Elect. Power Energy Syst.*, vol. 98, pp. 362–372, Jun. 2018.

[16] M. Amin and M. Molinas, "Small-signal stability assessment of power electronics based power systems: A discussion of impedance- and eigenvalue-based methods," *IEEE Trans. Ind. Appl.*, vol. 53, no. 5, pp. 5014–5030, Sep. 2017.

[17] C. Guo, A. Zheng, Z. Yin, and C. Zhao, "Small-signal stability of hybrid multi-terminal HVDC system," *Int. J. Electr. Power Energy Syst.*, vol. 109, pp. 434–443, Jul. 2019.

[18] X. Chen, Y. Liang, G. Wang, H. Li, B. Li, and Z. Guo, "A control parameter analysis method based on a transfer function matrix of hybrid multi-terminal HVDC system with flexible adaptability for different operation modes," *Int. J. Electr. Power Energy Syst.*, vol. 116, Mar. 2020, Art. no. 105584.

[19] Z. Hai-lin, Y. Shu-Jun, and Z. Peng, "Research on small-signal stability of hybrid multi-terminal HVDC system and control system parameter design," *J. Eng.*, vol. 2017, no. 13, pp. 2401–2406, Jan. 2017.
[20] H.-J. Kim, S.-W. Kang, G.-S. Seo, P. Jang, and B.-H. Cho, "Large-signal stability analysis of DC power system with shunt active damper," *IEEE Trans. Ind. Electron.*, vol. 63, no. 10, pp. 6270–6280, Oct. 2016.
[21] P. Manohar, V. Kelamane, D. Kaushik, and W. Ahmed, "Improved controls for LCC-VSC hybrid HVDC system," in *Proc. Int. Conf. Circuits, Controls Commun. (CCUBE)*, Bengaluru, Indian, 2013, pp. 1–5.
[22] E. Prieto-Araujo, A. Egea-Alvarez, S. Fekriasl, and O. Gomis-Bellmunt, "DC voltage droop control design for multiterminal HVDC systems considering AC and DC grid dynamics," *IEEE Trans. Power Del.*, vol. 31, no. 2, pp. 575–585, Apr. 2016.
[23] M. Huang, Y. Peng, C. K. Tse, Y. Liu, J. Sun, and X. Zha, "Bifurcation and large-signal stability analysis of three-phase voltage source converter under grid voltage dips," *IEEE Trans. Power Electron.*, vol. 32, no. 11, pp. 8868–8879, Nov. 2017.
[24] J. O. Flower, "The topology of the mixed potential function," *Proc. IEEE*, vol. 56, no. 10, pp. 1721–1722, Oct. 1968.

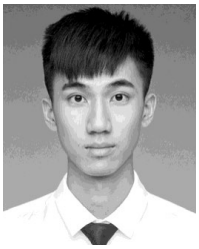

BINGKUN LI received the B.E. degree in electrical engineering from the South China University of Technology, Guangzhou, China, in 2018, where he is currently pursuing the master's degree in electrical engineering. His research interests include control and protection for HVDC systems, and high-voltage direct current technology.

YUANSHENG LIANG received the Ph.D. degree in electrical engineering and automation from the South China University of Technology, Guangzhou, China, in 2008. He is currently an Associate Professor with the School of Electric Power Engineering, South China University of Technology. His research interests include protection, fault location, and automation of electric power systems.

GANG WANG received the Ph.D. degree in electrical engineering and automation from Tianjin University, Tianjin, China, in 1998. He is currently a Professor with the School of Electric Power Engineering, South China University of Technology. He is the Director of the Power Engineering and Technology Research and Development Center, Guangdong, China. His major research interests include power system protection and control, fault analysis, power system planning and reliability, and high-voltage direct current technology.

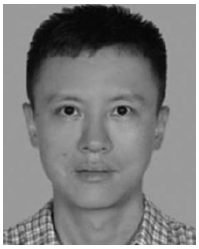

HAIFENG LI received the Ph.D. degree in electrical engineering and automation from the South China University of Technology, Guangzhou, China, in 2004. He is currently an Associate Professor with the School of Electric Power Engineering, South China University of Technology. His major research interests include power system protection and control, smart distribution networks, and high-voltage direct current technology.

XINQUAN CHEN received the B.E. degree in electrical engineering from the South China University of Technology, Guangzhou, China, in 2018, where he is currently pursuing the master's degree in electrical engineering. His research interests include protection, fault location, and high-voltage direct current technology.